Circumglobal Teleconnection in the Northern Hemisphere Summer*

QINGHUA DING AND BIN WANG+

Department of Meteorology, School of Ocean and Earth Science and Technology, University of Hawaii at Manoa, Honolulu, Hawaii

(Manuscript received 20 September 2004, in final form 1 February 2005)

ABSTRACT

Analysis of the 56-yr NCEP–NCAR reanalysis data reveals a recurrent circumglobal teleconnection (CGT) pattern in the summertime midlatitude circulation of the Northern Hemisphere. This pattern represents the second leading empirical orthogonal function of interannual variability of the upper-tropospheric circulation. The CGT, having a zonal wavenumber-5 structure, is primarily positioned within a waveguide that is associated with the westerly jet stream. The spatial phases of CGT tend to lock to preferred longitudes. The geographically phase-locked patterns bear close similarity during June, August, and September, but the pattern in July shows shorter wavelengths in the North Pacific–North America sector. The CGT is accompanied by significant rainfall and surface air temperature anomalies in the continental regions of western Europe, European Russia, India, east Asia, and North America. This implies that the CGT may be a source of climate variability and predictability in the above-mentioned midlatitude regions.

The CGT has significant correlations with the Indian summer monsoon (ISM) and El Niño–Southern Oscillation (ENSO). However, in normal ISM years the CGT–ENSO correlation disappears; on the other hand, in the absence of El Niño or La Niña, the CGT–ISM correlation remains significant. It is suggested that the ISM acts as a "conductor" connecting the CGT and ENSO. When the interaction between the ISM and ENSO is active, ENSO may influence northern China via the ISM and the CGT. Additionally, the variability of the CGT has no significant association with the Arctic Oscillation and the variability of the western North Pacific summer monsoon. The circulation of the wave train shows a barotropic structure everywhere except the cell located to the northwest of India, where a baroclinic circulation structure dominates. Two possible scenarios are proposed. The abnormal ISM may excite an anomalous west-central Asian high and downstream Rossby wave train extending to the North Pacific and North America. On the other hand, a wave train that is excited in the jet exit region of the North Atlantic may affect the west-central Asian high and, thus, the intensity of the ISM. It is hypothesized that the interaction between the global wave train and the ISM heat source may be instrumental in maintaining the boreal summer CGT.

1. Introduction

The word "teleconnection" has been commonly used to describe relationships in the low-frequency variability of the tropical and extratropical atmospheric circulations, precipitation, and temperatures, especially those related to the mature phases of El Niño–Southern Oscillation (ENSO) during boreal winter (Trenberth et al. 1998). Using orthogonally rotated principal component analysis and the teleconnectivity method, a number of prominent teleconnection patterns have been identified in the Northern Hemisphere (NH) extratropics throughout the year (e.g., Wallace and Gutzler 1981; Mo and Livezey 1986; Barnston and Livezey 1987, among others). Some of these teleconnection patterns show a regional scale with a wavelike structure.

The Asian summer monsoon is a dominant feature of the NH summer circulation. Teleconnection patterns that are associated with the Asian summer monsoon have received increasing attention in recent decades. A significant positive correlation in summer rainfall between India and northern China has been noted on the interannual time scales (Liang 1988; Guo and Wang

* School of Ocean and Earth Science and Technology Contribution Number 6583 and International Pacific Research Center Contribution Number 329.

+ Additional affiliation: International Pacific Research Center, School of Ocean and Earth Science and Technology, University of Hawaii at Manoa, Honolulu, Hawaii.

Corresponding author address: Mr. Qinghua Ding, Department of Meteorology, University of Hawaii at Manoa, 2525 Correa Road, Honolulu, HI 96822.
E-mail: qinghua@hawaii.edu

1988; Kripalani and Singh 1993; Kripalani and Kulkarni 1997, 2001; Zhang 1999). In these two regions, floods and droughts often concur in tandem. In addition, summer rainfall variations over southern Japan are found to negatively correlate with the Indian rainfall variations, in particular, during the early summer (Kripalani and Kulkarni 2001; Krishnan and Sugi 2001). Several studies have shown that in the strong Indian summer monsoon (ISM) years there are two equivalent barotropic anticyclonic anomalies occurring over the middle latitudes of the Eurasian continent. One is located to the west of the Tibetan Plateau, and the other is over northeast Asia (Wang et al. 2001; Krishnan and Sugi 2001; Wu and Wang 2002). They speculated that the upstream anticyclonic anomaly results from the sensible heat flux associated with the prominent surface temperature anomalies over the Tibetan Plateau, while the downstream anticyclone over northeast Asia accounts for the increased rainfall in northern China and decreased rainfall in southern Japan. The linkage between the ISM and east Asian summer monsoon (EASM) rainfall anomalies is established through large-scale circulation anomalies over midlatitude Asia.

It is also noted that this teleconnection over Eurasia connecting the ISM and EASM is a portion of a global-scale wave train linking Asia and North America (Wang et al. 2001). In a study of the principal modes of interannual variations over the U.S. summer rainfall, Lau and Weng (2002) found that the first two empirical orthogonal functions (EOFs) are both linked to a wave train pattern starting from east Asia. They named one of the teleconnections the "Tokyo–Chicago express" (Lau et al. 2004a).

During May, a large-amplitude stationary Rossby wave train that was induced by the heat sources in the Bay of Bengal was noted by Joseph and Srinivasan (1999). In July, a teleconnection pattern, which emanates from North Africa to east Asia along the midlatitude westerly jet, was described by Lu et al. (2002). They suggested that this route further links to the subtropical heating anomalies over the Atlantic. In August, Enomoto et al. (2003) proposed that the Bonin high (an equivalent barotropic, warm-core anticyclone south of Japan) forms as a result of the propagation of stationary Rossby wave energy along the east Asian jet. They named this pattern the "silk road" teleconnection.

During the northern summer the teleconnection patterns are weaker than its winter counterpart, and the local teleconnection patterns appear to be disconnected. The aforementioned teleconnection studies mainly focused on the teleconnection pattern confined to the Eurasian or the Asia–Pacific–North America sectors. A question that arises is whether these regional teleconnections are linked with each other or are independent from each other. This study aims at addressing this question. We will show evidence that a circumglobal teleconnection (CGT) exists during the NH summer and on interannual variability. The ISM–EASM teleconnection, the silk road, and the Tokyo–Chicago express are regional manifestations of the CGT pattern that is recurrent in the NH summer.

Another motivation of this study is to investigate the relationship between the summertime westerly jet stream and the NH summer CGT. Hoskins and Ambrizzi (1993) pointed out that the structure of the basic flow might put a strong constraint on the Rossby wave path. The large vorticity gradients that are associated with the jet stream can form a waveguide with a limited meridional dimension, confining wave activity to a zonal band and transporting it downstream a long distance before it is dispersed. In a recent study, Branstator (2002) documented a NH winter circumglobal teleconnection pattern that was trapped in the jet stream waveguide. Evidence also indicates that the variability of the east Asian jet stream is associated with the Asian–Pacific–American winter climate (Yang et al. 2002).

The possible impacts of this CGT on the interannual variability of precipitation and surface temperature, and their possible feedback on the CGT, are another major concern of the present investigation. To understand the cause of the CGT, we will investigate its relationship with the surface boundary conditions and other major modes of climate variability in the NH. Specific questions that will be addressed include the following: 1) How does the CGT vary from June to September? 2) How does the CGT affect the rainfall distribution over different continental regions of the NH? 3) How is the CGT associated with global sea surface and land surface temperature anomalies? 4) Are there any connections between this CGT pattern and other major mode of climate variability, such as ENSO, the Arctic Oscillation (AO), and the western North Pacific summer monsoon (WNPSM) variability? Adequately addressing these questions may provide valuable insights into the establishment and maintenance of the CGT. Based on our analysis, a hypothesis about the mechanism of the CGT is proposed.

2. Data and method

The major dataset that is used is the National Centers for Environmental Prediction–National Center for Atmospheric Research (NCEP–NCAR) reanalysis data from 1948 to 2003 (Kalnay et al. 1996). The monthly

global SST for the period of 1948–2003 is taken from the National Oceanic and Atmospheric Administration (NOAA) extended reconstructed SST (ERSST), provided by the NOAA–Cooperative Institute for Research in Environmental Sciences (CIRES) Climate Diagnostics Center.

Three datasets of station observations were used for our analyses: 1) a long, homogeneous all-Indian summer [June–July–August–September (JJAS)] rainfall index for the period of 1948–98, and the monthly rainfall for the same period in 29 subdivisions of India (Parthasarathy et al. 1994); 2) the monthly precipitation dataset of 160 weather stations in China from January 1951 to December 1999, compiled by the Chinese Meteorological Administration; and 3) the precipitation/surface air temperature dataset with land-only coverage from 1950 to 1999, assembled by the University of Delaware from the Global Historical Climate Network (GHCN) and, more extensively, from the archive of Legates and Willmott (1990a,b).

To focus on year-to-year variations, throughout the paper, the interannual component of the data was used. The long-term trend and decadal variations with a period longer than 8 yr are removed using Fourier harmonic analysis of the monthly or seasonal mean anomalies.

A simple composite technique is used to derive teleconnection patterns with reference to a well-defined index. The method of a composite provides information about both the spatial distribution and quantitative estimation of the amplitudes of anomalies. In all of the cases studied here, we found that the two sets of composites, with respect to the selected extremely positive and negative circumglobal teleconnection index (CGTI) scenarios, are nearly a mirror image of each other. Therefore, it suffices to examine the circulation anomaly difference between positive and negative composite for each summer month. The composite positive-minus-negative CGTI will be simply interpreted as positive CGTI anomalies.

The composite algorithm is as follows. An atmospheric variable is first averaged over those periods when the CGTI falls below -0.8 standard deviations. This average is then subtracted from the average over those periods when the CGTI exceeds 0.8 standard deviations. A Student's t test was used to assess the statistical significance of the differences between positive and negative composites (Wilks 1995).

3. CGT pattern

Figure 1a shows the standard deviation of summer (June–September) mean 200-hPa heights. The most prominent center of variability is located over the northeast Atlantic and western Europe in the exit region of the North Atlantic jets. Other successive centers of maximum variability are observed over west-central Asia (37.5°N, 65°E), from east Asia to the Gulf of Alaska, and northern North America. Of note is that these variability centers are closely associated with the major summertime jet streams or are located in the downstream jet exit region.

The region that exhibits large variability to the northwest of India corresponds to the upstream anomalous circulation center of the ISM–EASM teleconnection (Wang et al. 2001). In view of the important role of the Asian summer monsoon in driving the NH summer circulation, and to assess the association between this Asian summer monsoon action center and the global atmosphere, we constructed a one-point correlation map of 200-hPa geopotential height anomalies with reference to the geopotential height over west-central Asia (35°–40°N, 60°–70°E), that is, in Uzbekistan and east Turkmenistan.

The most striking feature that is shown by the one-point correlation map (Fig. 1b) is that the pressure variations over the northeast Atlantic–western Europe, northeast Asia, North Pacific, and North America are all nearly in phase with the variations over west-central Asia, as shown by the significant positive correlations. In contrast, the pressure fluctuation over European Russia, upstream of the reference area, exhibits a significant negative correlation. The spatial distribution of the correlations in Fig. 1b is quite similar to the ISM–EASM teleconnection that is shown by the composite map in Fig. 8 of Wang et al. (2001), suggesting that the ISM–EASM teleconnection is one portion of the global teleconnection, consisting of a successive pressure trough and ridge circling all longitudes from Eurasia to North America and the North Atlantic. When the reference point is moved to the aforementioned positive correlation center, in each case, the correlation map yields the similar global wave train pattern (shown in Fig. 1b), with five anomalous high pressure (ridge) centers being "fixed" in the same location (figures not shown).

The quasi-zonal alignment of the anomalous high pressure (or ridge) centers is primarily confined to 35°–45°N. The CGT pattern has approximately a zonal wavenumber-5 structure. Hereafter, the term "CGT," borrowed from Branstator (2002), is used to describe this global zonal wavenumber-5 teleconnection pattern with six prominent "centers of action" over western Europe, European Russia, west-central Asia, east Asia, the North Pacific, and North America, as

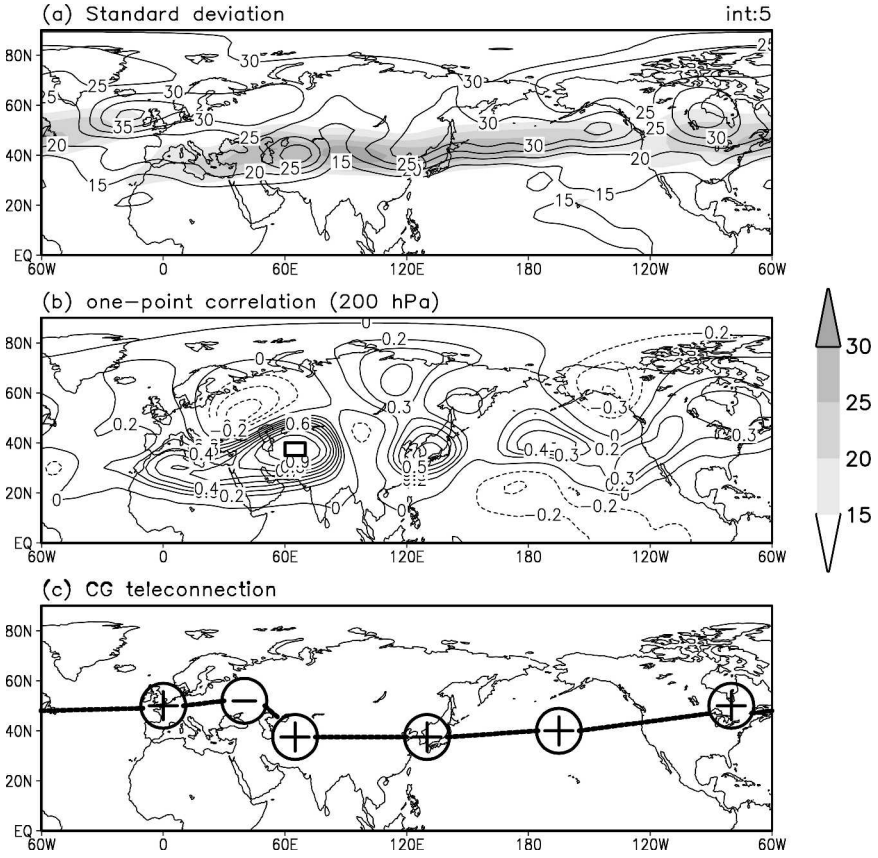

FIG. 1. (a) Standard deviation of summer (JJAS) 200-hPa NH heights (contour) and climatological 200-hPa jet stream (zonal wind) with the magnitude greater than 15 m s^{-1} (shading) for the period of 1948–2003. (b) One-point correlation map between the base-point (box) and summertime (JJAS) 200-hPa geopotential height for 1948–2003. (c) Schematic illustrating six main action centers of the CGT.

represented by "+" and "−" in the schematic diagram in Fig. 1c.

For convenience of discussion a CGTI is defined by using the interannual variability of the 200-hPa geopotential height averaged over the reference area to the northwest of India (west-central Asia) (35°–40°N, 60°–70°E). These indices are made of either monthly or seasonal mean anomalies; both are normalized by their corresponding standard deviation. Thus, the sign of CGT is positive during months when a ridge sits over west-central Asia.

Figure 2 is presented to show the sensitivity of the CGT pattern to the choice of the location where the CGTI is defined. Because of the broad region of high correlation with the CGTI in the vicinity of the base point (Fig. 2a), two extra one-point correlations were recalculated with the reference area located at the westernmost (37.5°N, 45°E in Fig. 2b) and easternmost (37.5°N, 80°E in Fig. 2c) boundary of the area that is circled by the contour of the correlation coefficient of 0.8. The similarity of the geographical distributions of the wave train patterns in the three correlation maps lends confidence to the robustness of the CGT, suggesting that the CGT is insensitive to the change of the index location in the region ranging from 45° to 80°E. However, beyond this region, the circumglobal features of the correlation map fade away and are replaced by ill-organized, sporadic maximum correlation centers (figures not shown). This indicates that the variability of summertime midlatitude flow tends to be composed of a zonal wavenumber-5 feature, with favored longitudes for each variability center.

4. Interpretation of the CGT

To determine whether the CGT is the primary mode of interannual variability of the NH troposphere, an EOF analysis of the temporal covariance matrix is performed using the seasonal (JJAS) mean 200-hPa geopotential height field. EOFs were computed over the

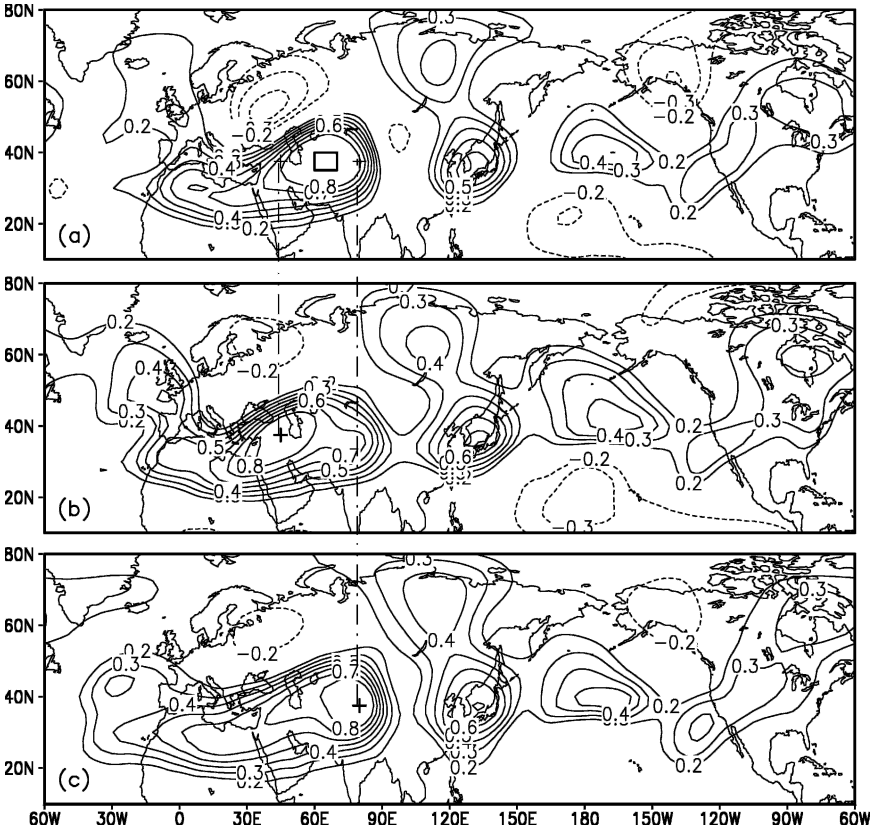

FIG. 2. One-point correlation maps showing the correlation coefficient between the 200-hPa height at base points (a) 35°–40°N, 60°–70°E, (b) 37.5°N, 45°E, and (c) 37.5°N, 80°E, and 200-hPa height at NH for 1948–2003.

entire NH, with the data weighted by the square root of the cosine of latitude to ensure that an equal area has the same contribution to the total variance. The significance and uniqueness of the EOFs that are tested by the Monte Carlo procedure (Preisendorfer 1988), and the rule of thumb that is derived by North et al. (1982), are illustrated in Fig. 3. The first two dominant modes, accounting for 21% and 14% of the total variance, respectively, are well separated from the other modes and are much greater than the Monte Carlo 99% criterion. However, the other modes have significantly overlapping error bars. We will, therefore, concentrate our attention on these two leading EOFs, whose spatial structure is given in Fig. 4. The corresponding precipitation and SST distribution are also obtained by correlating the time series of each principal component (PC) with the seasonal precipitation anomalies over land and seasonal SST anomalies between 70°N and 30°S.

The first EOF mode features a zonally oriented band of above-normal height near 50°N, extending from east Asia across the entire North Pacific. The below-normal height belt covering the entire tropical area is obvious to the south of 20°N. The SST that is associated with this EOF mode (Fig. 4c) exhibits a strong cold anomaly tendency over the entire equatorial region, with a maximum negative value over the Indian Ocean basin. The only exception is a narrow half-circle band straddling the west Pacific, where the weaker positive value dominates.

The second EOF mode, accounting for 14% of the variance, bears a strong resemblance to the CGT in its spatial structure and the locations of the five positive centers. The pattern correlation coefficients, measuring the spatial correlation between the two fields (Figs. 2a and 4b), are 0.74 with a sample size up to a total number of grids (144 × 73). The PC time series of the second EOF has a correlation coefficient of 0.6 with the CGTI. In view of these strong correlations with the CGT, it is suggested that the CGT represents the second leading mode of the low-frequency variability of the NH atmosphere during summer.

Compared to the absence of a significant correlation that is associated with EOF-1, the correlation coefficient between the time series of EOF-2 and rainfall

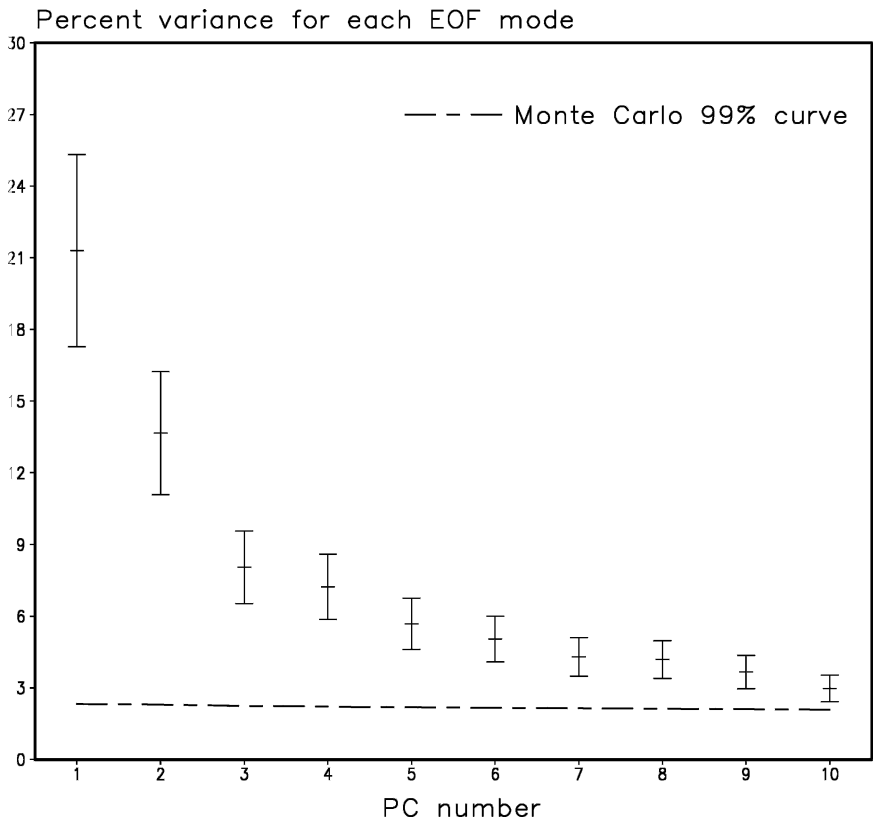

FIG. 3. EOF structure for seasonal (JJAS) 200-hPa geopotential height anomalies in terms of the total variance explained by each EOF for their respective interannual time series. Error bars are determined by the formula of North et al. (1982). The Monte Carlo 99% curve is based on the method of Preisendorfer (1988).

anomalies over northwest India reaches 0.6, and that in the northern China is 0.5. In addition, a significant negative correlation was found over western Europe, central Asia, and North America. The correlation between the CGTI and precipitation/SST anomaly (SSTA) reveals a similar pattern to that shown in Fig. 4d. Although the CGT is not the primary mode of interannual variability of the NH atmosphere, it may provide useful information about the climate variability and predictability in the global scale.

The negative correlation between the anomalous SST and time series of EOF-2 in the eastern equatorial Pacific (Fig. 4d), accompanied with the well-known surrounding "horseshoe" pattern with a positive correlation on the north, west, and south, corresponds to a La Niña event. The coupling between the elongated warm SST zone and anticyclone vortex aloft is also found over the west-northern Pacific. The coexistence of the EOF-2 mode and La Niña event indicates the possible contribution of ENSO in modulating the CGT. This aspect will be reexamined later in the discussion of the ENSO–CGT relationship (section 6c).

5. Subseasonal variation of the CGT

To better understand the structure and dynamical processes that are responsible for the CGT, teleconnection patterns in each summer month (June–September) are examined to help identify subseasonal variations of the CGT. Using the CGTI for an individual month, the year-to-year monthly data can be grouped into two categories: the years with strong positive anomalies to the northwest of India and the years with a strong negative anomaly. To deduce the dominant patterns of multilevel circulation change over the NH related to the fluctuation of the CGTI, ridge-minus-trough composite maps of the upper-, mid-, and the low-level geopotential heights are calculated.

Figures 5–6 show the composite maps at two levels (200, 700 hPa) for June, July, August, and September, respectively. The 500- (figure not shown) and 200-hPa levels (Fig. 5) have very similar patterns, but the amplitude increases with height. Overall, from June to September, the global-scale wave train of alternating low and high geopotential anomalies with considerable

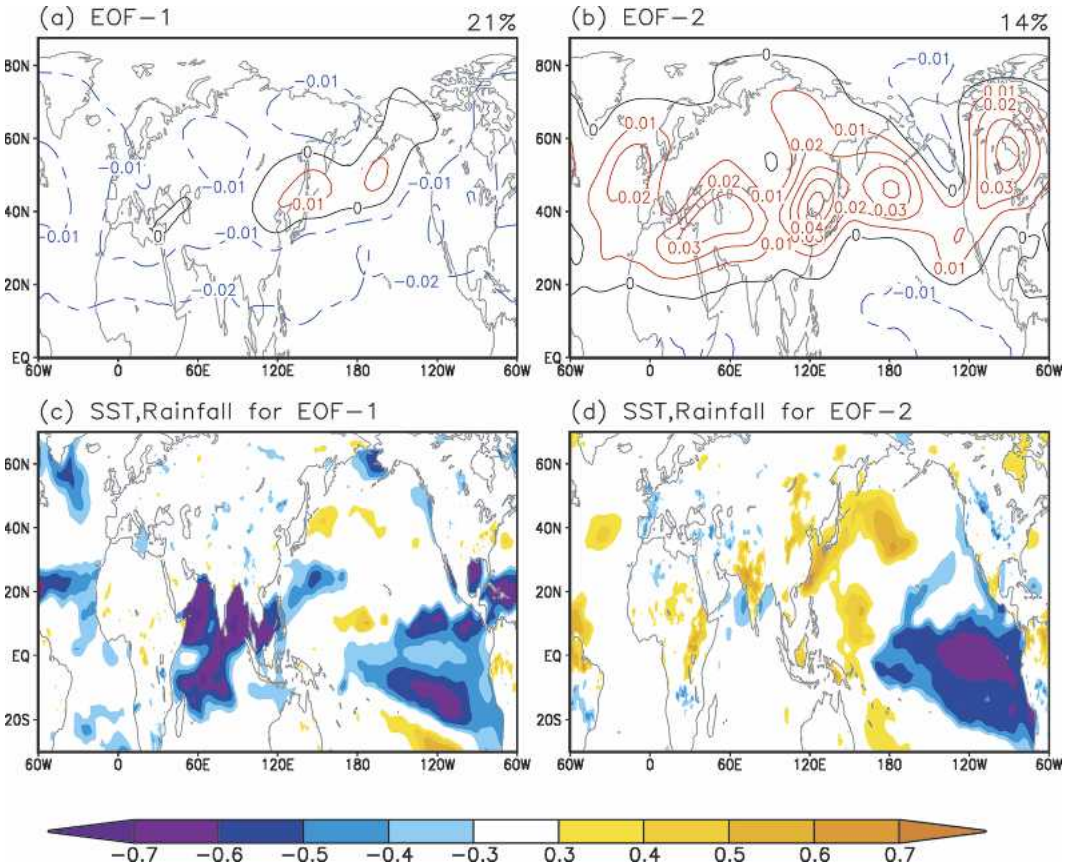

FIG. 4. First two modes of an EOF analysis applied to NCEP–NCAR reanalysis seasonal (JJAS) geopotential height anomalies at 200 hPa. (a) The first mode explained 21% of total variance; (b) the second mode associated with the CGT explained 14% of total variance. (c) Correlation coefficient between the time series of EOF-1 and Delaware precipitation data over land and ERSST over ocean. (d) Correlation coefficient between the time series of EOF-2 and Delaware precipitation data over land and ERSST over ocean.

intensity extends from Eurasia to North America along 30°–50°N. The main positive centers of the wave train in June, August, and September tend to be fixed at several regions, such as west-central Asia, east Asia, North Pacific, and the central United States, but the positive center over the Atlantic and western Europe seem to be more variable in location and intensity. The negative anomalies are found in between these five high centers.

Note that the CGT patterns are best defined in August when the strongest linkage between the Atlantic and central Asia exist. The September pattern is similar to the August one except for the intensities at their corresponding centers. The June pattern also closely resembles the August pattern, except for the height anomalies over the Atlantic. The July pattern, however, bears close resemblance to the August pattern only from North Africa and across Eurasia. From the North Pacific to the North Atlantic, the July pattern features shorter wavelengths, so that the circulation anomalies reversed phases compared to the other 3 months.

The lower-level composites (Fig. 6) show that nearly all of the teleconnection cells have a barotropic structure, except for the upper-level anomalous ridge to the northwest of India, which has a tilted baroclinic structure with a lower-level-enhanced cyclonic anomaly over the Arabian Peninsula and adjacent sea. It is conceivable that the equivalent barotropic circulation anomalies along the CGT pattern have significant influence on the local climate system and the corresponding precipitation and temperature fields in each month.

6. Climate anomalies associated with the CGT

a. Rainfall anomalies

The composite precipitation anomalies that are associated with the extreme values of the CGTI indicate that during the high-index phase of CGTI, several re-

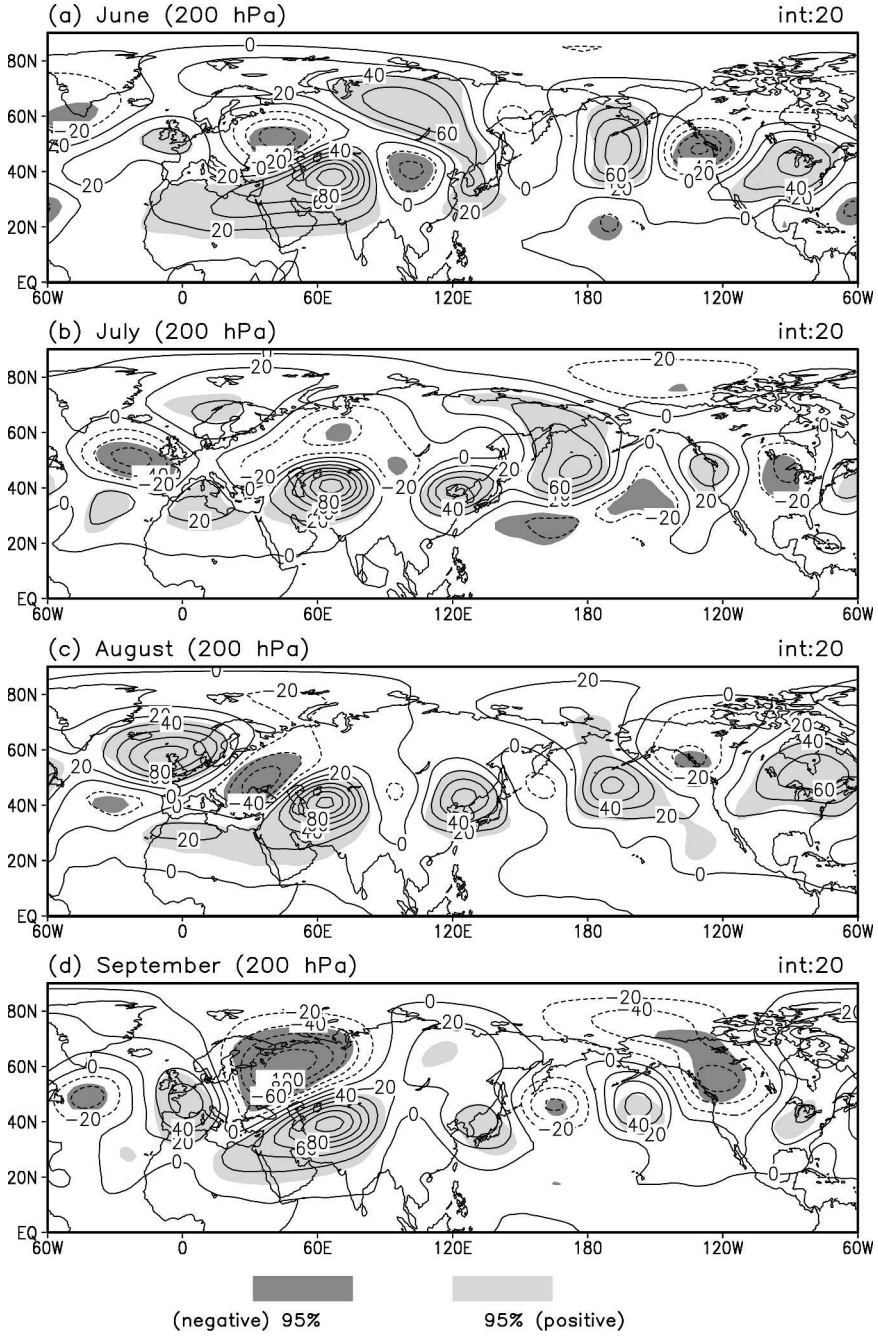

FIG. 5. Composite difference of geopotential height at 200 hPa between positive and negative CGTI years for (a) Jun, (b) Jul, (c) Aug, and (d) Sep, respectively. Light shading denotes regions of difference at 95% confidence level with a positive value, and heavy shading denotes regions of difference at 95% confidence level with a negative value. Contour intervals are 20 m (. . . , −40, −20, 0, 20, 40, . . .).

gions show significant precipitation anomalies. In each of these regions, the precipitation anomalies that are associated with the high CGTI exhibit opposite signs with those derived for the low-index phase. Thus, to a first approximation, the precipitation anomalies in these regions are linearly related to the phase of the CGTI. Thus, the ridge-minus-trough composite of the CGTI will represent the strong CGTI case.

Based on land-covered global precipitation compiled by Legates and Willmott (1990a,b; Delaware precipita-

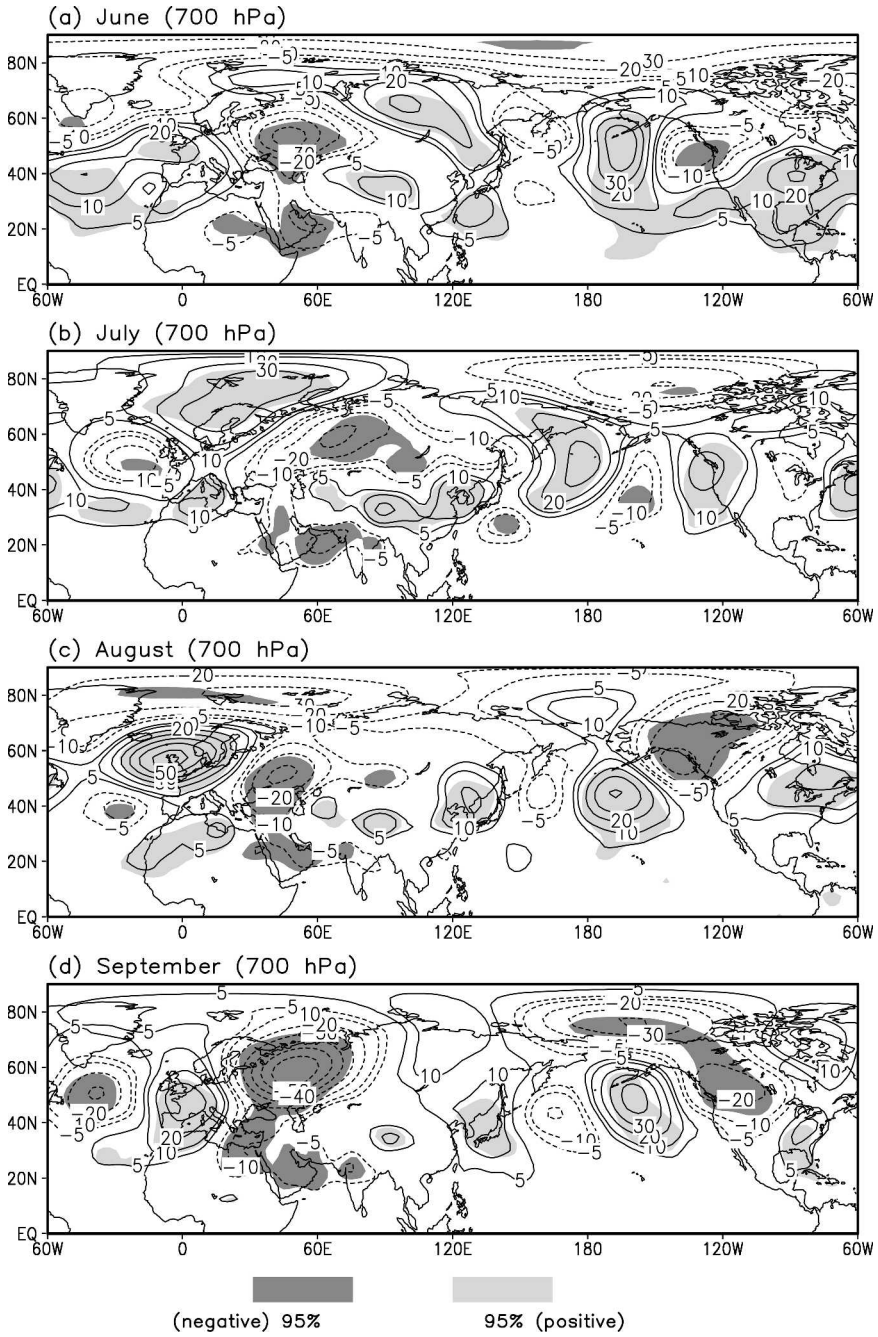

FIG. 6. Same as Fig. 5, except for 700 hPa. Contour intervals are 10 m (. . . , −30, −20, −10, −5, 5, 10, 20, 30, . . .).

tion data), the ridge-minus-trough composite maps with respect to the CGTI for each month are presented in Fig. 7. To test the reliability of the Delaware data, we also present the composite precipitation anomalies that are obtained from Chinese and Indian station rainfall measurements by using the same procedure. The grand consistency between the global and the local station data suggests the high quality and reliability of the Delaware global precipitation dataset.

A common feature from June to September is the enhanced precipitation in the ISM over northwest India and Pakistan when there is a strong upper-level positive height anomaly over west-central Asia. Based on the baroclinic structure of the local circulation anomaly as-

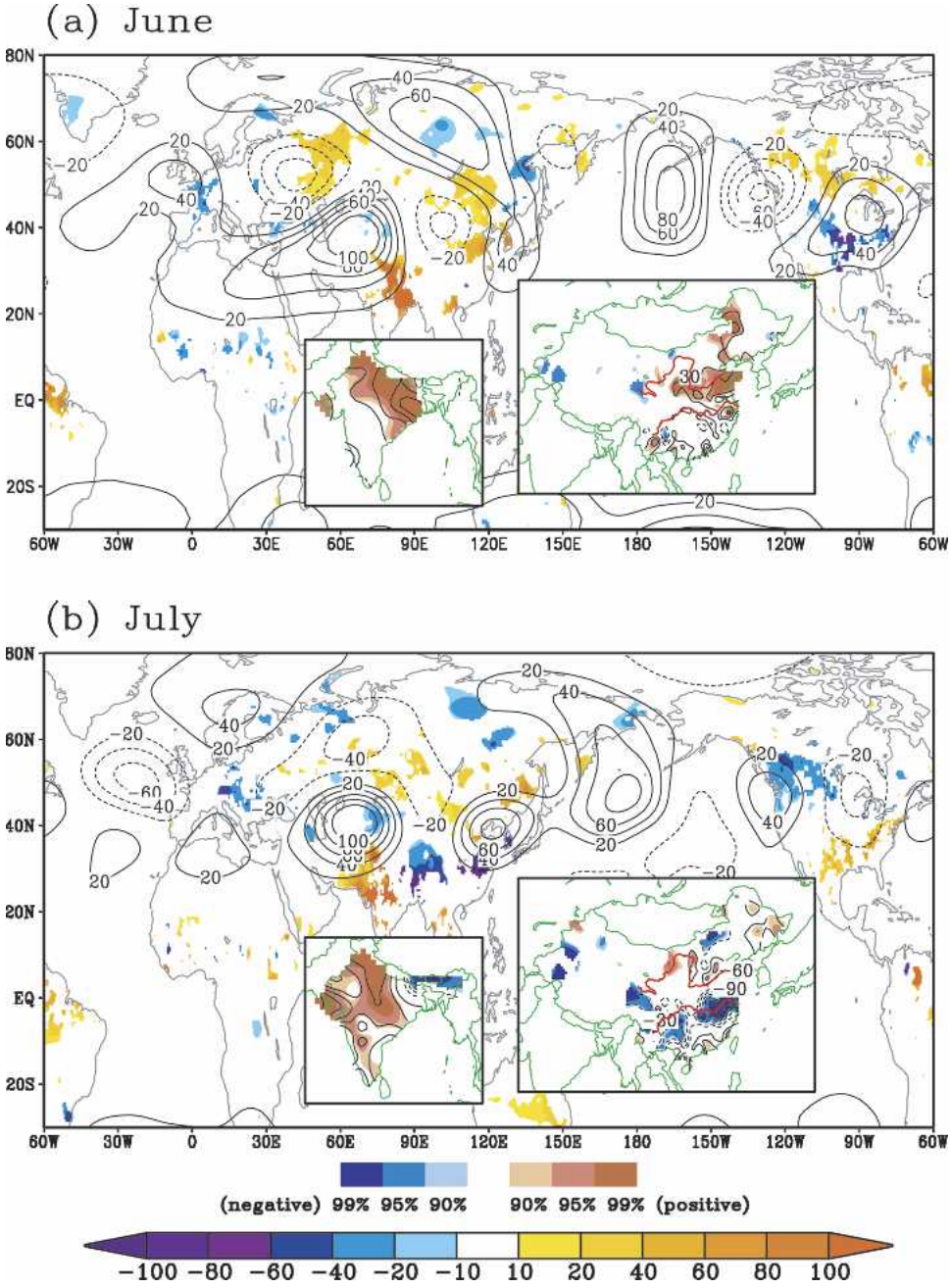

FIG. 7. Composite difference of Delaware global precipitation (background map) and station precipitation (small map) between positive and negative CGTI years for (a) Jun, (b) Jul, (c) Aug, and (d) Sep. Differences (mm month^{-1}) above 90% statistical significance level are shown by shading in global map. The corresponding CGT from Fig. 5 is shown as contour. For India and China station data, red shading denotes regions of difference at 90%, 95%, and 99% confidence levels with a positive value, and blue shading denotes regions of difference at 90%, 95%, and 99% confidence levels with a negative value. Contour intervals are 30 mm month^{-1} (. . . , −60, −30, 30, 60, . . .).

sociated with the precipitation anomaly (section 5), the important effect of monsoon heating in generating this Gill-type Rossby wave pattern in the northwest was inferred (Gill 1980; Rodwell and Hoskins 1996; Joseph and Srinivasan 1999; Wang et al. 2001; Enomoto et al. 2003). It is possible that the teleconnection pattern is, in part, the response of the midlatitude westerlies to the ISM heat source.

As seen in Fig. 7, significant precipitation anomalies are also found over midlatitude Eurasia and North

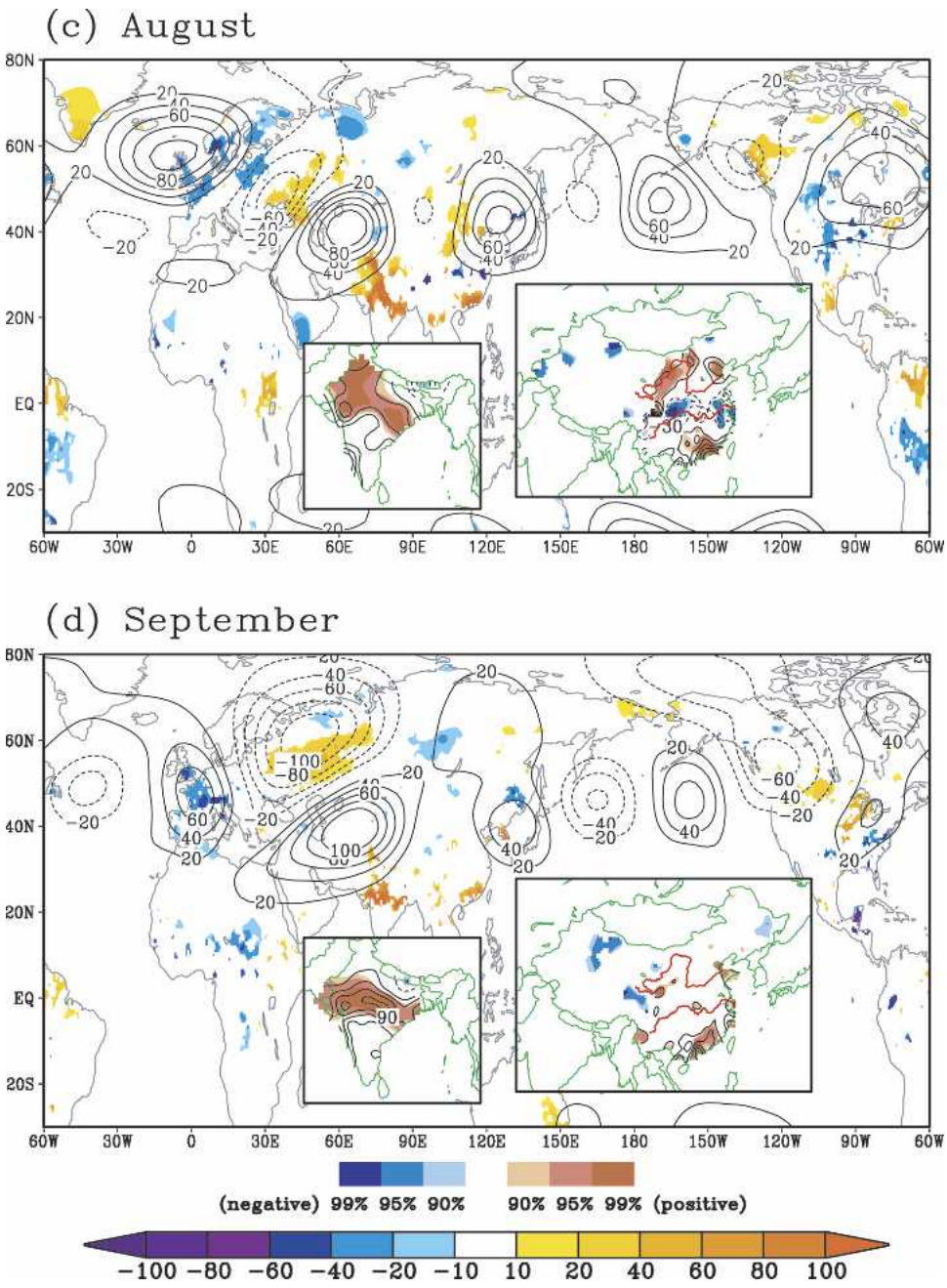

FIG. 7. (*Continued*)

America. They are well associated with the strong action centers of the circulation counterpart shown by the contours in the global map.

Deficient precipitation regions occur over central western Europe in each summer month, but the negative anomaly centers shift their locations and change their intensities from month to month. There is also a positive precipitation anomaly region occurring in eastern Europe to the north and west of the Caspian Sea during June, August, and September, with the largest spatial coverage and maximum intensity occurring in September.

Over North America, the patterns are more variable from month to month, but a northwest–southeast oriented dipole appears to be a recurrent pattern, especially in July, August, and September. The Great Plains region is affected the most. The polarity of the precipitation anomalies in July tend to be out of phase with other months, in accord with the changes in the teleconnection phase in the corresponding atmospheric cir-

culation anomalies between July and the other 3 months.

Because the anticyclonic vortex of the CGT over east Asia progresses northward from June to August and withdraws in September, the east Asia rainfall anomalies exhibit somewhat complex structures. There is, however, a general tendency that increased rainfall occurs over northern China along the Yellow River Valley, particularly in June and August. In July and August when the major precipitation band is located over northern China (Ding 1992), the region of the Yangtze River Valley experiences deficient monsoon rainfall. In August and September, the rainfall in the southeast coast of China is evidently enhanced.

From the foregoing analysis, it is seen that a connection among the changes of precipitation over western Europe, European Russia, south Asia, east Asia, and North America is established in association with the atmospheric CGT anomalies. In general, when northwest India and Pakistan experience floods, there is a drought tendency over central Western or north Europe, and a wet tendency in eastern Europe (an European dipole). Meanwhile, over east Asia a north–south dipole pattern tends to occur with enhanced precipitation in northern China and reduced precipitation in the Yangtze River Valley. Over North America, a north–south oriented seesaw anomaly pattern concurs in June, and there is a northwest–southeast dipole in July, August, and September. The locations and signs of the polarity centers, however, vary. The simultaneous change of precipitation over east Asia and North America during the summer season agrees with the findings of Lau and Weng (2002). The primary mode of the east Asia–Midwest U.S. teleconnection and associated rainfall anomalies (Fig. 6 in Lau and Weng 2002) resembles the negative phase of the CGT over the Pacific sector during July (Figs. 5b and 7b), while the secondary mode is similar to the CGT structures occurring in other months. This resemblance suggests that the well-documented teleconnection between east Asia and the Midwest United States is a part of the CGT over the NH.

As previously indicated, the buildup and maintenance of the equivalent barotropic anomalous vortex of teleconnection is the key process in linking the precipitation change over different locations of the NH on the interannual time scale. Here, an attempt is made to examine the detailed process. To see a significant example, attention was paid to the moisture transport over the east Asian monsoon region during August, on account of the strong rainfall anomalies over northern China.

Figure 8 shows the positive-minus-negative CGTI composite field of the moisture transport that is integrated from the surface to 300 hPa in August. The contour indicates the divergence of the anomalous water vapor flux. A clockwise moisture flux vortex dominates over northeast Asia. On the south side of the cell, a strong easterly moisture flow over lower reaches of the Yangtze River Valley splits into two streams near 30°N, 110°E. The northern component turns southeasterly to converge over northeast China; the southern component turns southwestward to provide sufficient moisture to the southeast coast of China. Previously, it was argued by Zhang (1999) that the increased moisture over northern China mainly came from the excessive moisture of the Bay of Bengal, and this kind of in-phase variation induces the linkage of the rainfall over the two areas. However, this is not the case for August. In August, the origin of the anomalous moisture in northern China primarily comes from the western Pacific. In summary, when the anomalous high is established over northeast Asia, it blocks the eastward-moving upstream troughs, which are most favorable for the occurrence of heavy rainfalls, inducing excessive rainfall to the west of the anomalous high. Meantime, a southeasterly airflow at its southern flank transports extra moisture into the middle range of the Yellow River Valley. If there were a typhoon to the south of the anomalous high, the easterly airflow would be further intensified and maintained longer (Ding 1994).

Similarly, over other areas, the equivalent barotropic circulation anomalies of the CGT are also responsible for excessive or deficient rainfall along its path through

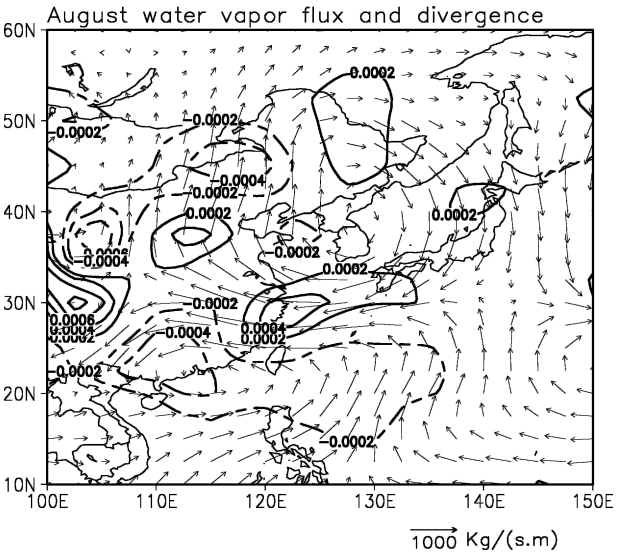

FIG. 8. Aug composite difference of water vapor transportation (1000–300 hPa) between positive and negative CGTI years. The divergence of water vapor transportation is plotted in contour.

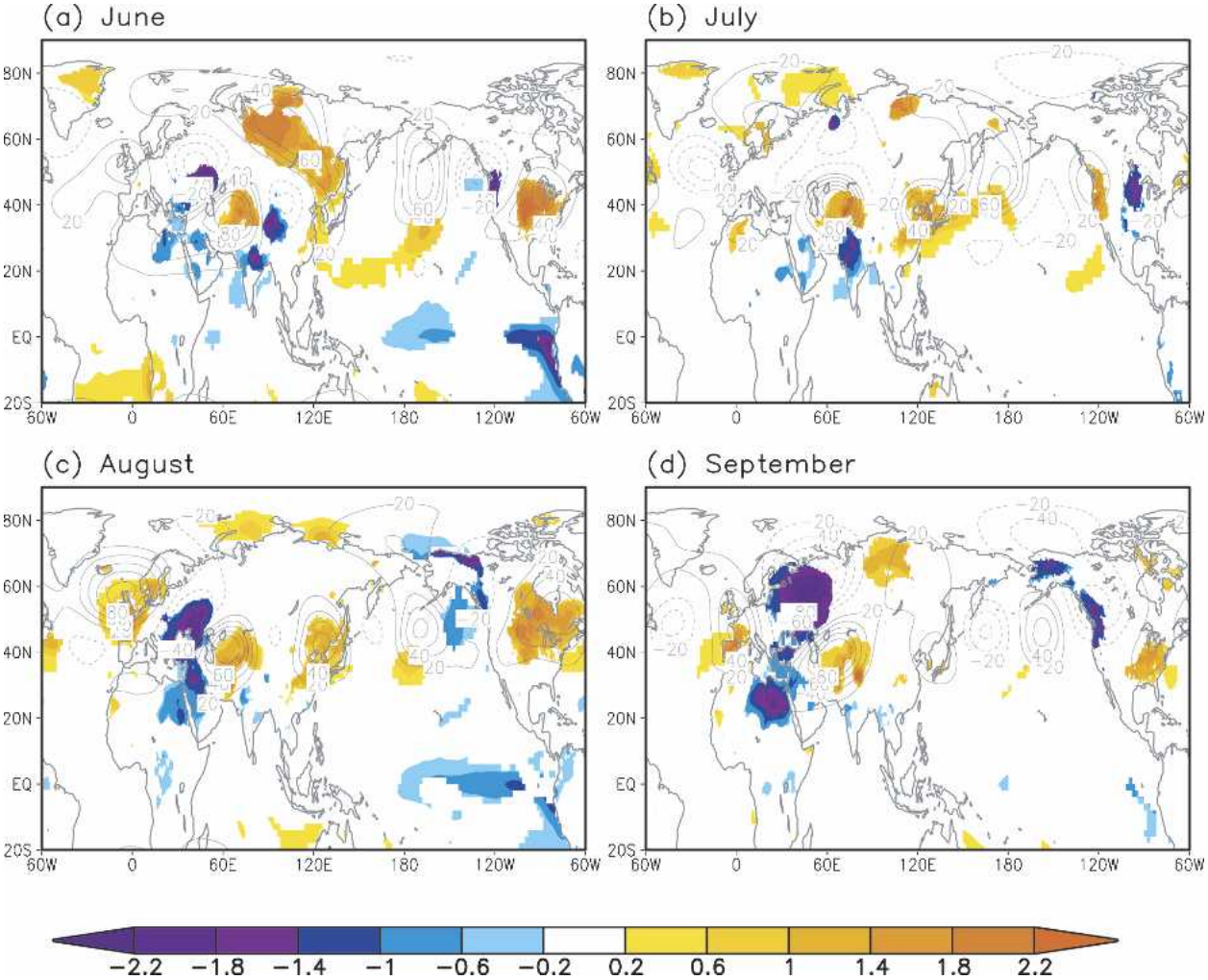

FIG. 9. Composite difference of Delaware global surface air temperature (over the land) and ERSST (over the ocean) between positive and negative CGTI years for (a) Jun, (b) Jul, (c) Aug, and (d) Sep. Differences above 95% statistical significance level are shown by shading. The corresponding CGT from Fig. 5 is shown as contour.

moisture advection and induced vertical motion. However, the reason for the covariability of the ISM and baroclinic circulation anomalies to the northwest of India is uncertain, but it could be related to an interaction between the ISM and midlatitude westerly flow.

b. Surface air temperature anomalies distribution

In the same format as that of Fig. 7, the temperature composite maps with somewhat more noticeable anomalies are shown in Fig. 9. The major structure of the CGT is also superimposed to show great coherence between the anomalous high (low) pressure and surface warming (cooling) along the track of the CGT. For example, corresponding to the anomalous anticyclonic circulation from west-central Asia to North America, above-normal temperature is found over the Pamir Plateau in each month, but also over northeast Asia from June to August and North America in June, August, and September. A reverse of the temperature anomalies in July occurs over the central United States. Because of the existence of the pressure anomaly with a barotropic structure, the shortwave radiation fluctuation that is associated with increased or decreased rainfall or cloud coverage may play a central role in generating the surface temperature change.

c. CGT is independent of ENSO

While the EOF analysis has demonstrated the significant correlations (−0.6) between the seasonal mean SST anomaly and time series of the EOF-2 mode over the eastern equatorial Pacific, in July and September, the concurrence of the CGT and La Niña event is non-

existent in the composite map (Figs. 9b,d) at the 95% confidence level, even at lower statistical criteria (90%) for the two-sample Student's *t* test. On the contrary, the La Niña signal is evident with moderate magnitude in June and August. Given the persistence of the eastern Pacific SSTA from month to month, if the CGT is excited by ENSO-related SST variation, one should not expect the discontinuity of the relationship between the CGT and ENSO anomalies. Therefore, it is inferred that the ENSO is unlikely a primary cause of the CGT.

To back up this point, we further computed the partial correlation in this subsection. For the 52-yr period, the correlation coefficient between the seasonal (JJAS) mean CGTI and the All-Indian Rainfall Index (AIRI) is 0.69; the correlation coefficient between the AIRI versus Niño-3 SST is −0.52; and the correlation coefficient between the CGTI and Niño-3 SST is −0.43. While the latter is statistically significant, because of the high correlation between the AIRI and Niño-3 index, it is plausible that ENSO may be correlated with the CGTI through its relation with the ISM. To test this idea, a partial correlation between the CGTI and Niño-3 SST index is computed by removing the CGTI–AIRI correlation. The partial correlation between the CGTI and Niño-3 SST reduces to −0.12. It suggests that the simultaneous relationship between the CGTI and ENSO activities results largely from the correlation between the ISM and CGTI. On the other hand, using monthly and seasonal data, the time-lag correlation with the Niño-3 SST anomaly leading CGTI by various lags (up to 9 month) did not reveal any significant lag relationship between the two indices.

Simply from the calculation of the partial correlation, we would expect that the ISM is more crucial than ENSO in controlling the CGT. The one-point correlation map between the seasonal CGTI and 200-hPa circulation anomalies for a non-ENSO year and non-ISM year, as shown in Fig. 10, confirms this conjecture. The ENSO year is defined as the developing phase of an ENSO event, based on Niño-3 SST anomalies. A total of 24 ENSO years (12 El Niño and 12 La Niña episodes, listed in Table 1) were identified. In the non-ENSO cases, these ENSO years were removed from the 56-yr time series when calculating the one-point correlation. With the same approach, 24 ISM years (12 strong ISM and 12 weak ISM years, listed in Table 1) that are characterized by the AIRI are eliminated in a non-ISM case. As shown in Fig. 10a, the structure of the CGT remains intact as ENSO is excluded, suggesting that the CGT exists independent of ENSO and that the induced precipitation anomalies are significant over Eurasia and North America. However, in the absence of the ISM (Fig. 10b), the CGT pattern and associated precipitation anomalies nearly completely vanish.

Alternatively, the EOF-2 of the seasonal mean 200-hPa height anomalies in a non-ENSO year captures the main structure of the CGT and corresponding rainfall variability (Fig. 10c). The similarity of the leading EOFs and equivalent percent variance for each mode between a non-ENSO year and the entire period (Fig. 4) suggests that the moderate magnitude of the SSTA over the eastern equatorial Pacific during the developing phase of an ENSO event is trivial for the summertime midlatitude circulation fluctuation in the NH. In contrast, in a non-ISM year, the CGT mode is not the dominant EOF of the NH atmosphere. The large distinctions in the formation of the CGT between non-ENSO and non-ISM years indeed prove that the CGT is closely related with the ISM instead of ENSO.

Given the strong linkage between ENSO and the ISM (13 out of 24 ENSO years are also ISM years in Table 1, and vice versa), it is possible that ENSO exerts an influence on the midlatitude rainfall variability through the ISM. This idea can be used to explain the coherence between the ENSO-developing phase and large summer rainfall anomalies in northern China (Wu et al. 2003; Feng and Hu 2004). When comparing the El Niño–La Niña composite map, (Figs. 11a,b), the prominent rainfall anomalies show the dry (wet) tendency over northern China and India in El Niño (La Niña) episodes, and the CGT-like circulation anomalies are nearly mirror images over Eurasia and the North Pacific, indicating the indirect effect of ENSO conveyed to northern China by the ISM, as well as the CGT. Because the CGT is not sufficiently strong to extend into North America (Fig. 11c), the precipitation anomaly is negligible over the continent, suggesting that the local climate is not sensitive to the adjacent SSTA over the eastern equatorial Pacific. Instead, it might be more easily influenced by the remote forcing from the ISM (Figs. 10a,b).

7. Discussion

a. Waveguide effect

Several key points have emerged from the previous analysis concerning the physical mechanism of the CGT that is involved with the ISM and westerly jets. Hoskins and Ambrizzi (1993) emphasized that strong westerly jets, acting as Rossby waveguides, have a tendency to enhance the geographical amplitude of low-frequency fluctuations. Ambrizzi et al. (1995) extended the theoretical work to the boreal summer case, and revealed the North African–Asian jet and the North Atlantic jet waveguide. The apparent propagation from the exit of

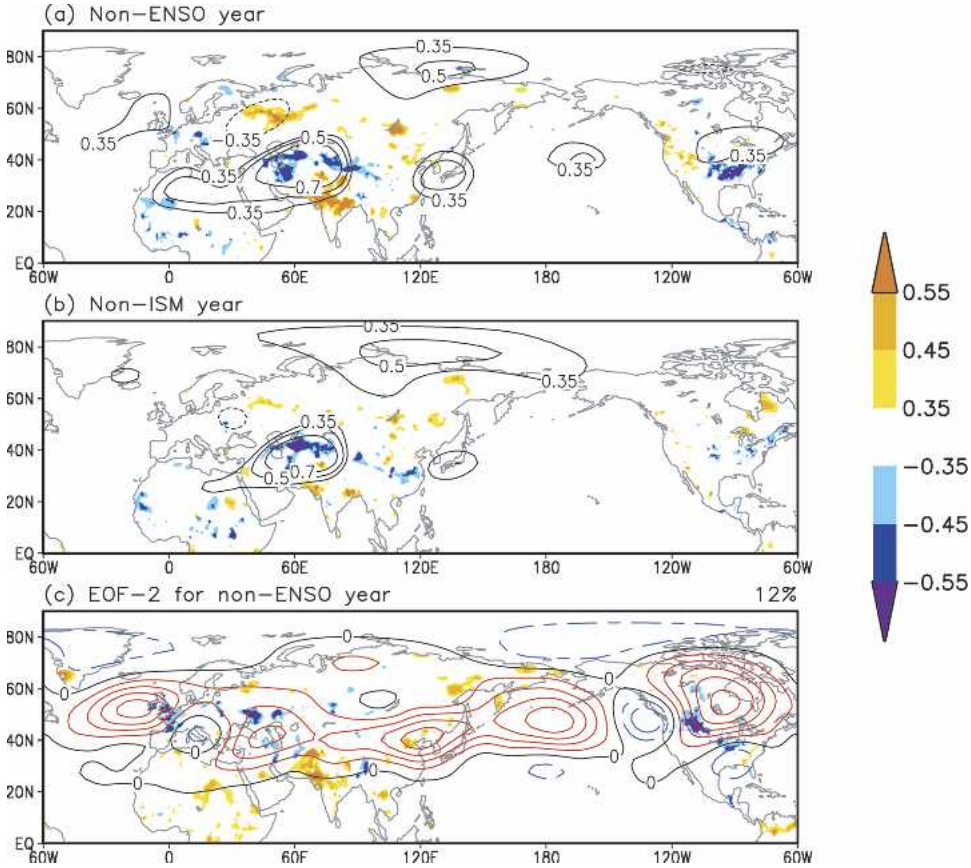

FIG. 10. One-point correlation map between the seasonal (JJAS) CGTI and 200-hPa geopotential height (contour) and Delaware global precipitation (shading) for (a) a non-ENSO year and (b) a non-ISM year. The contour and shading denotes the significant correlation above 95% confidence level (±0.35). (c) EOF-2 of seasonal (JJAS) geopotential height anomalies at 200 hPa for a non-ENSO year. EOF-2 associated with the CGT explained 12% of total variance. The significant (above 95% confidence level) correlation coefficient between time series of EOF-2 and Delaware precipitation data is shown as shading.

one jet stream to the entrance of the other connects the two, and establishes a waveguide spiraling around the whole latitudinal circle around 40°N.

To illustrate a combined view (Fig. 12), the climatological zonal wind (200 hPa) and the CGT for each month are displayed together. From June to July, a northward jump of the westerly jet from 35° to 40°N takes place abruptly. Closely related with the position of the climatological westerly jet flow in each month, the Rossby wave train is established and the wave energy propagates along the waveguide to downstream regions. This is revealed by the coincidence between the cell of the teleconnection pattern and the jet stream in each month.

Main anomalous heat source regions are also identified from the distribution of the ISM rainfall anomaly (filled circle in Fig. 12). The zero lines of the 200-hPa zonal wind are marked by the dotted lines. It is seen that the monsoon heat source anomaly is generally located at the edge of the midlatitude westerlies during each month, and the tropospheric divergent winds that are induced by the strong upward motion (figures not

TABLE 1. El Niño, La Niña, strong ISM, and weak ISM years for the non-ENSO and non-ISM correlation analysis during 1948–2003. A year that is both an ENSO and ISM year is boldfaced. ENSO defined according to Niño-3 SST; the ISM defined according to AIRI.

El Niño	**1957**, 1963, **1965**, 1969, **1972**, 1976, **1982**, 1986, **1987**, 1991, 1997, **2002**
La Niña	**1949**, 1954, 1955, **1964**, **1967**, **1970**, **1973**, **1975**, 1984, **1988**, 1998, 1999
Strong ISM	**1949**, 1956, 1961, **1964**, **1967**, **1970**, **1973**, **1975**, 1983, **1988**, 1990, 1994
Weak ISM	1951, 1952, **1957**, 1960, **1965**, **1972**, 1974, 1979, **1982**, **1987**, 1992, **2002**

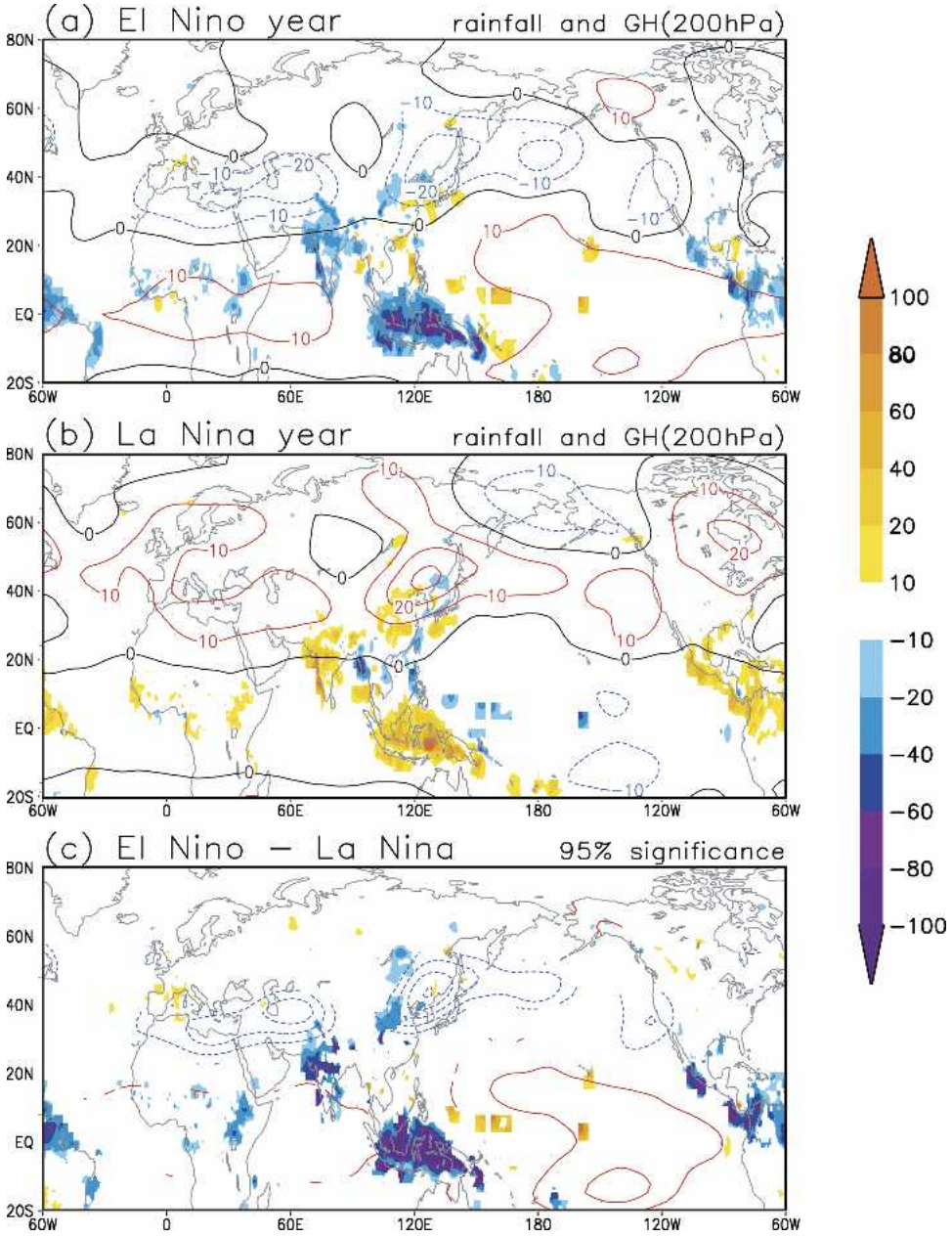

FIG. 11. Composite of seasonal (JJAS) 200-hPa height (contour) and Delaware global precipitation (shading; mm month^{-1}) anomalies for (a) El Niño and (b) La Niña events, during 1948–2003. Definitions of El Niño and La Niña year are based on Table 1. (c) The significant (95% level by Student's t test) difference between El Niño and La Niña composites is shown.

shown) located in the midlatitude westerlies can generate Rossby wave trains (Hoskins and Karoly 1981; Sardeshmukh and Hoskins 1988).

The stationary Rossby wavenumber (K_s) of the 200-hPa basic flows is calculated using an idealized theoretical model (Hoskins and Ambrizzi 1993). For June–September, the governing total wavenumber K_s along the jet stream varies from 6 to 8 (Fig. 13). According to the width of the waveguide, the meridional wavenumber is estimated to be 5. Thus, the deduced zonal wavenumber of the stationary Rossby waves are about 5 along the circumglobal waveguide. Evidently, this result is in good agreement with the observed prominent zonal wavenumber-5 structure of the CGT. An exception to this is July's relatively weak waveguide over the North Pacific and North American sector, where the

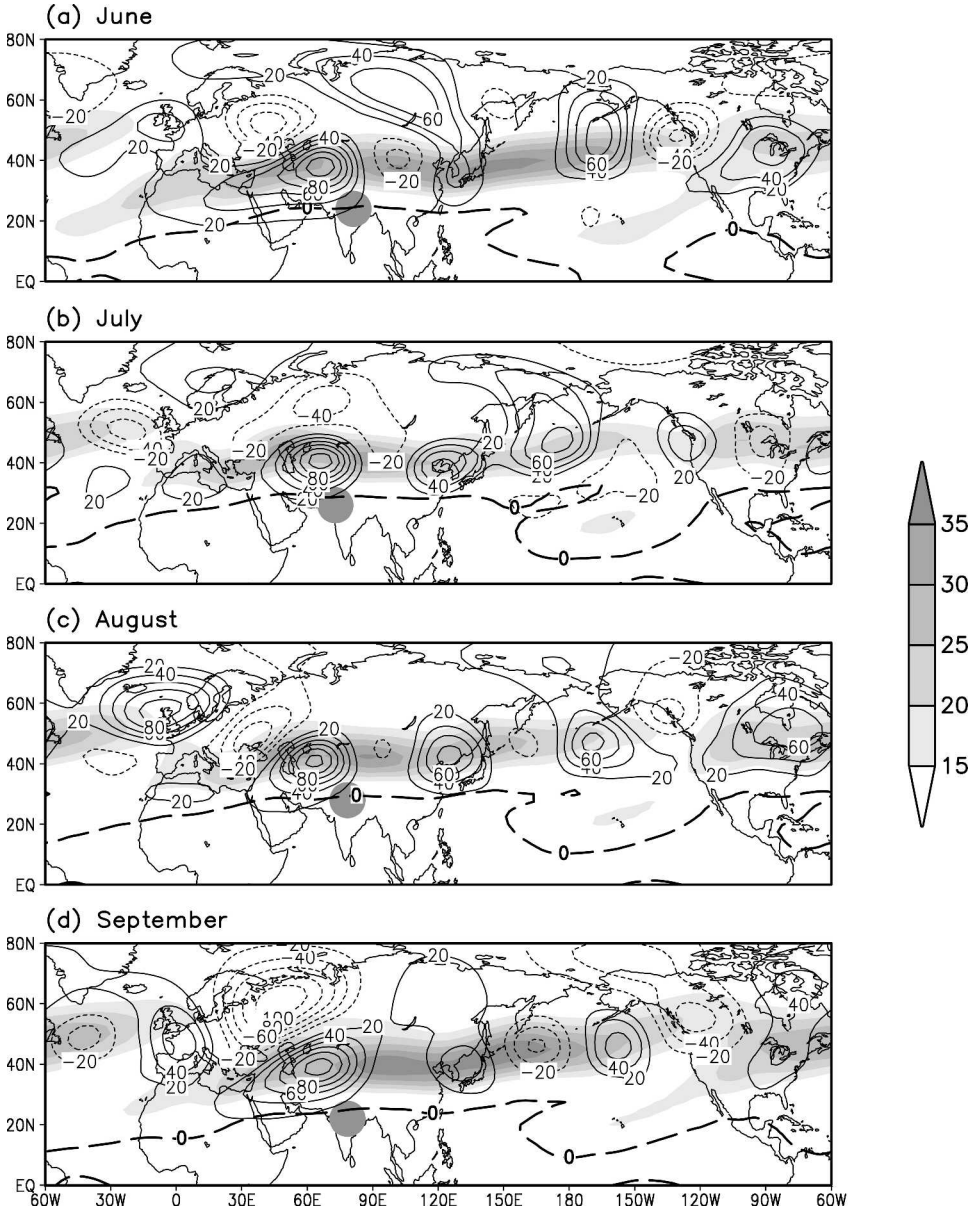

FIG. 12. Combined picture showing the major 200-hPa circulation anomalies (contour; derived from Fig. 5) accompanied with climatological 200-hPa zonal wind (shading; greater than 15 m s^{-1}) from Jun to Sep. The dotted line indicates the zero zonal wind line at 200 hPa. Over India, the composite difference of India rainfall (derived from Fig. 7) is denoted by a filled circle.

estimated total wavenumber is larger than that observed in other 3 months. This explains the shorter wavelength of the CGT from Japan to the Atlantic during July.

b. Role of internal dynamics of the basic state

So far we have considered the ISM as a primary forcing to the teleconnection. However, a wavelike upstream circulation anomaly, particularly in August and September, can be traced back from west-central Asia to western Europe, even to the Atlantic Ocean, which suggests that the ISM is not the only source for the CGT. Upstream influences from Europe and the Atlantic Ocean are also possible. Evidence has been presented that the potential effect of the midlatitudes on the Tropics is considerable (Liebmann and Hartmann 1984).

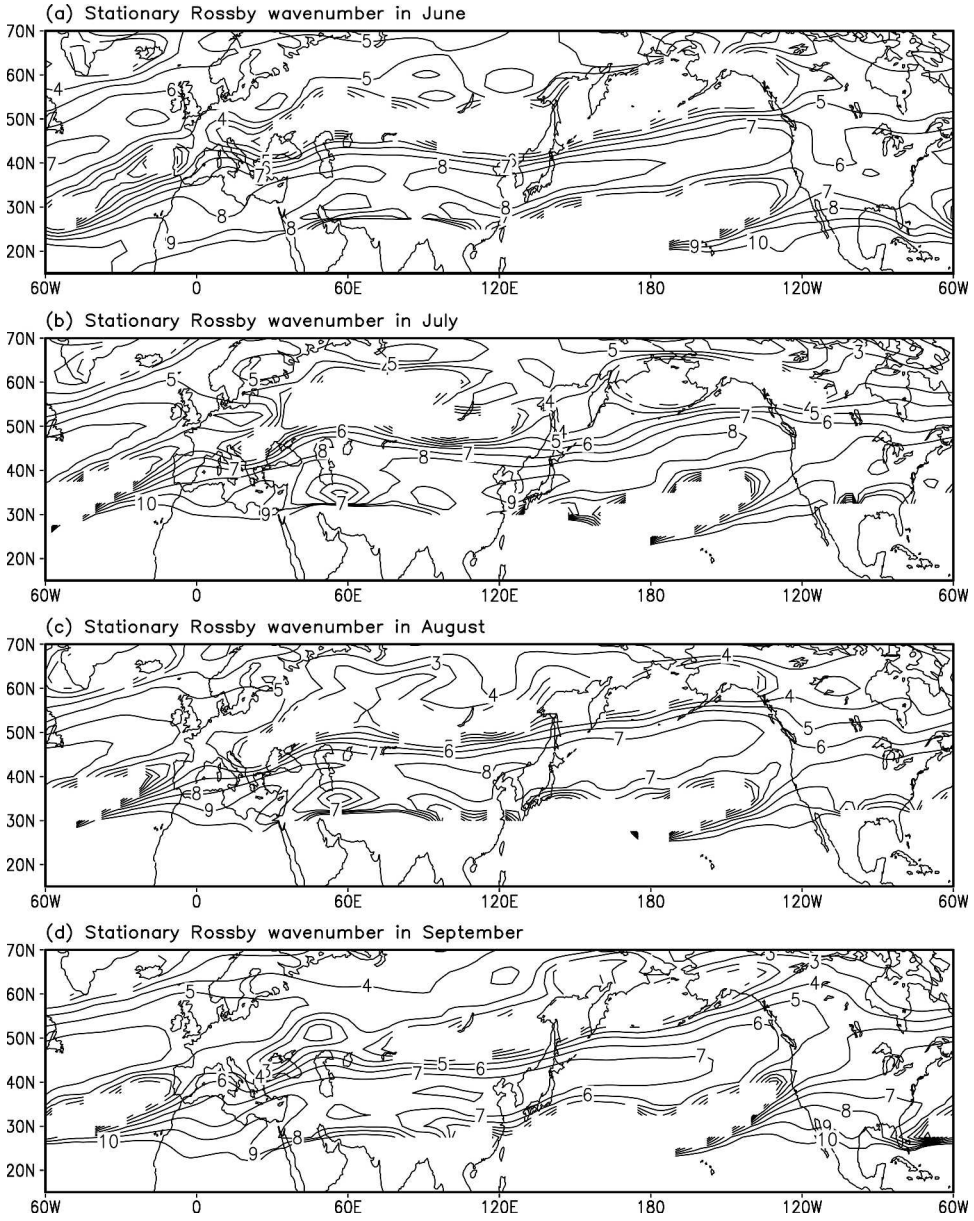

FIG. 13. Based on climatological 200-hPa zonal flow for the period of 1948–2003, the stationary Rossby wavenumbers, defined in Hoskins and Ambrizzi (1993), for (a) Jun, (b) Jul, (c) Aug, and (d) Sep.

Some previous studies have examined the influence of the mid- and high-latitude system on the break/active phase of the ISM on intraseasonal and interannual time scales (Ramaswamy 1962; Raman and Rao 1981; Krishnamurti et al. 1989; Kripalani et al. 1997). One of the earliest finding was reported by Raman and Rao (1981), who found that two upper-tropospheric blocking ridges are observed over the North Caspian Sea (55°N, 55°E) and eastern Siberia (50°N, 100°E) in the severe drought ISM year. Based on the synoptic charts of a "bad" monsoon year, they showed that the evolution of these two blocking highs have a close relationship with the break in the monsoon and the midlatitude wave activity moving eastward from west to east Asia. Kripalani et al. (1997) emphasized the role of the blocking ridge to the northwest of India as a signal of the active monsoon over north and central India. He also showed some evidence for an enhanced 500-hPa easterly flow to the north of India prior to the positive rainfall anomalies over India and the existence of the

stronger westerlies prior to and during negative rainfall anomalies. Interestingly, these results captured both the strong and weak CGTI phase of the CGT, and underlined the important role of the large-scale midlatitude flow in driving the rainfall anomalies over northern India.

The upstream wave train cannot be explained by the ISM forcing, because the Rossby wave dispersion that is associated with the ISM propagates eastward, and, thus, the wave activity that originated from the Atlantic and western Europe should be regarded as another factor to generate the CGT.

The circulation pattern shown in Fig. 5 appears to suggest that the action center over western Europe (50°N, 0°E) is a key area that emits an arching-shaped wave train migrating from Europe to west-central Asia via eastern Europe. It is important to bear in mind (based on Fig. 1a) that this key area is also located at the exit region of the North Atlantic jet stream, and the magnitude of the climatological standard deviation in this area is the largest in the NH. According to Simmons et al. (1983), during the winter the disturbance in the jet exit region can be readily excited by tropical forcing through barotropic energy conversions that are associated with both the meridional and zonal gradients of the basic state wind; the latter is particularly strong in the jet exit region, and this center is not very sensitive to the particular location of the heating. It is possible that the large atmospheric variability in this area is associated with the barotropic instability of the summer mean flow. Thus, a single strong variability center downstream the summertime North Atlantic westerly jet is possibly maintained, in part, by the efficient kinetic energy extraction from the basic state, and the upstream tropical or extratopical forcing along the jet can initiate this strong variability.

c. Connection between the CGT and the AO

Thompson and Wallace (2000) demonstrated that an "annular" structure mode, which is referred to as the AO, with opposing geopotential height fluctuations in the polar cap region and the surrounding zonal ring centered near 45°N, was favored in the wintertime NH. A recent study of Ogi et al. (2004) has found that the AO is also evident in the summer, but has a smaller meridional scale than its winter counterpart. Because both the CGT and AO exhibit a circumglobal feature over the midlatitudes, it is natural to ask "what is the relationship between these two low-frequency modes," although the CGT did not reveal any significant signal over the polar region.

Ogi et al. (2004) defined a summer (JJAS) AO index using time series of the leading mode obtained by applying an EOF analysis to the zonally averaged geopotential height field over the meridional vertical domain. The summer geopotential height anomalies at 200 hPa that are correlated with this index are shown in Fig. 14. A typical AO mode with a seesaw structure of geopotential height between the polar region and midlatitudes is apparent. Compared to the CGT, the midlatitude ring of the AO is closer to the Arctic Circle, with several strong centers over the Bering Sea, north Canada, and north Europe, respectively. The correlation coefficient between this index and the CGTI is 0.18, which is not significant at the 90% confidence level, suggesting some independence between the CGT and AO.

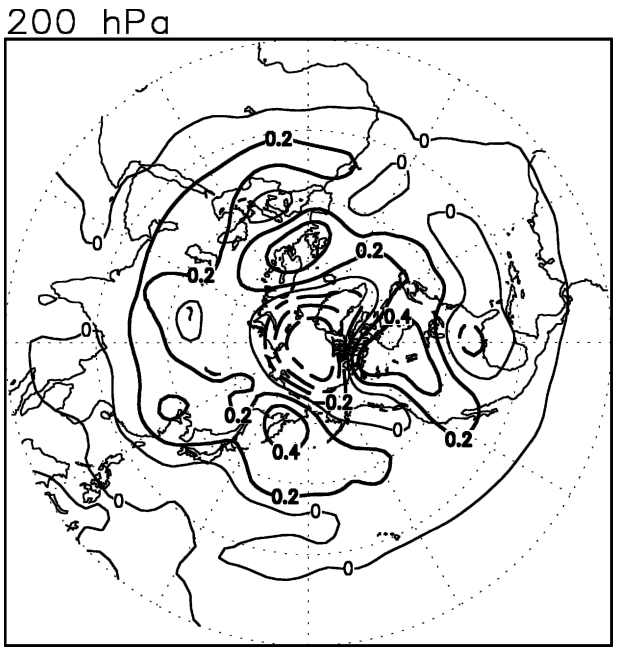

FIG. 14. Correlation coefficient of the seasonal mean (JJAS) 200-hPa geopotential height anomalies with the summer (JJAS) AO index. The index is obtained following the method of Ogi et al. (2004).

Alternatively, the other kind of AO index, defined by Thompson and Wallace (1998, 2000), is used to reproduce the simultaneous correlation for monthly data. This index, which is more widely accepted by the public and available to download from the Climate Prediction Center, is the principal components of the leading EOF of sea level pressure poleward of 20°N that is based on all months starting in 1950. The sole significant correlation (0.35) between the CGTI and AO index occurs in June, reflecting some degree of linkage between the two modes. The monthly AO index and CGTI time series were also cross correlated with a lag up to 1 yr, and no significant correlation was detected.

d. Connection between the CGT and the WNPSM

In addition to attempting to establish whether any connection exists between the CGT and ENSO or the AO, particular attention is devoted to determining whether the WNPSM has an influence on the CGT. Accordingly, the correlations between the monthly/seasonal CGTI and the corresponding WNPSM index defined by Wang and Fan (1999) are computed. The monthly/seasonal correlations yield very weak values and are insignificant at the 90% confidence level, indicating the decoupling of the WNPSM from the CGT.

The work of Lau (1992) has demonstrated that the teleconnection connecting east Asia to North America is associated with the normal mode of the northern summertime climatological flow. It seems that the latent heating in the western Pacific and the Indian Ocean regions can exert an influence on the generation of this unstable mode. However, in our study, a poor relationship between the WNPSM and the CGT is observed, and the significant baroclinic structure that is associated with tropical heating is only found near the Indian peninsula. Therefore, the strong ISM, especially the excessive rainfall over northwest India and Pakistan, could act as a trigger to provoke the normal mode of the basic flow straddling the North Pacific. Furthermore, the extratropical air–sea interaction between the atmospheric circulation and in situ SST is believed to be helpful in maintaining this system over the North Pacific (Wang et al. 2001; Lau et al. 2004b).

8. Summary

By using 56-yr NCEP–NCAR reanalysis data, we have documented the Northern Hemispheric summer atmospheric teleconnection on an interannual time scale. We identified a circumglobal standing oscillation in the planetary waves. The salient results of the present study are summarized below.

a. Conclusions

Based on a newly defined circulation index using the 200-hPa geopotential height anomalies averaged over west-central Asia (35°–40°N, 60°–70°E), a circumglobal teleconnection (CGT) with a preferred wavelength and longitudinal phase locking is documented for each month of the summer season (JJAS). The CGT is primarily confined within the waveguide that is associated with the NH summer jet stream. This teleconnection is similar to the EOF-2 mode of the interannual variability of the NH summer circulation. Most of the action centers of the CGT display a nearly equivalent barotropic structure, with a maximum amplitude at the upper troposphere. The only exception is the center of action located to the northwest of India, which exhibits a noticeable baroclinic structure, suggesting that the diabatic heating effect of Indian monsoon precipitation provides the maintenance of the CGT. In July, the CGT favors a shorter stationary wave downstream of Japan, and the teleconnection east of Japan seems to reverse its sign when compared to the pattern in other months.

The appearance of the climate anomalies in rainfall and surface air temperature over western Europe, European Russia, northwest India/Pakistan, east Asia, and North America reflects the footprints of the CGT and the role of CGT in linking regional climate variations along its path. The precipitation anomalies that are associated with the CGT are consistent with the rainfall anomaly patterns that are associated with the summertime ISM–EASM teleconnection and the east Asia–North America teleconnection, reported in the previous studies. Thus, these two well-known regional teleconnection patterns can be understood as the regional component of the CGT.

Generally speaking, a strong ISM tends to be accompanied by suppressed rainfall over Europe and above-normal rainfall in northern China and European Russia, whereas an out-of-phase anomaly pattern with a north–south seesaw structure is seen over America, whose phase varies from month to month. The reversed anomalous rainfall distribution for a weak ISM also holds, because the atmospheric circulation patterns that are associated with the strong and weak monsoon largely "mirror" each other.

Correlation analyses were preformed to investigate the relationships between the CGT and other climate anomaly patterns, such as ENSO, the AO, and the WNPSM. The partial correlation and composite analysis suggests that, in the absence of the ISM effect, the CGTI is not significantly correlated with ENSO, and the CGT pattern does not exist. In June, about 12% variability of the CGT overlaps the variability of the AO; however, in the other months, the covariance between the CGT and AO is scant. Furthermore, the relationship between the CGT and the WNPSM is also insignificant.

b. Hypothesis and speculations

Based on observational evidence, we propose that the maintenance of the CGT relies on an interaction between the CGT circulation and the ISM. Figure 15 highlights the major points of the hypothesis. The organization of the CGT in the upper troposphere can be viewed as taking place in two scenarios, which will be referred to as scenario I and II. For the first scenario,

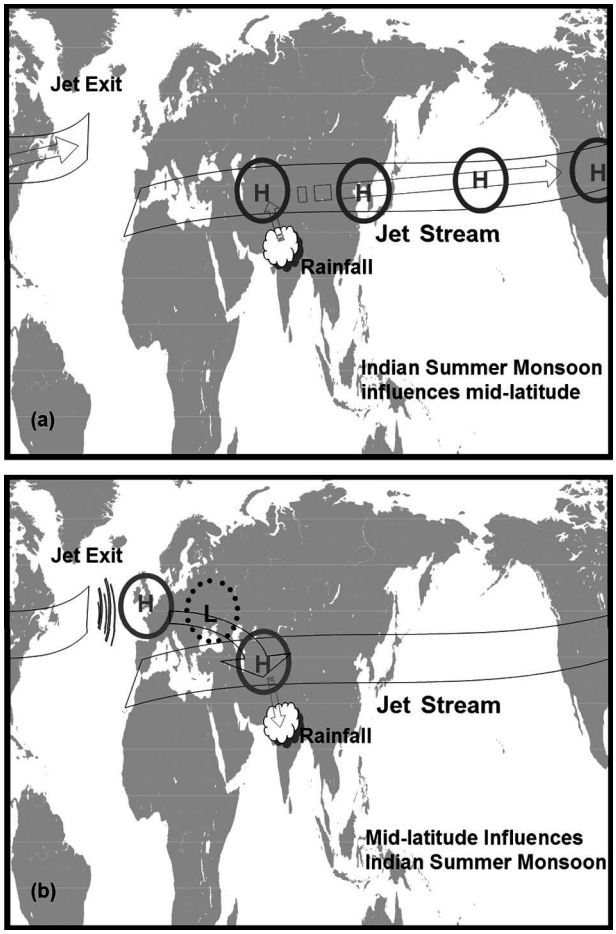

FIG. 15. Schematic diagram illustrating the entire mechanism of the CGT consisting of two scenarios during the positive phase of CGTI. The cloud denotes the strong ISM and the circles represent the CGT in the upper level.

the ISM plays a more active role in affecting the midlatitude atmosphere. An enhanced ISM initially generates an upper-level anomalous high to its northwest over west-central Asia, and then excites successive downstream cells along the waveguide through Rossby wave dispersion.

The second scenario is the means by which the barotropic instability of the westerly jet dominates, while the ISM plays a more passive role in receiving influences from midlatitude atmosphere. In the scenario II, as a result of the strong barotropic instability at the jet exit region in the North Atlantic, an anomalous high can be triggered over western Europe by the upstream disturbances. A Rossby wave train stretching from western Europe to west-central Asia is favored by the local basic state. Accompanying the wave train, strong stationary wave energy is transported from a high latitude to west-central Asia, inducing a secondary anomalous high. The passage of an upper-level anticyclonic anomaly to the northwest of India results in enhanced convection over northwest India and Pakistan through reinforcing the instability that is associated with the easterly jet. The latter mechanism is explained as follows. To the south of the anomalous high over west-central Asia, the easterly anomalies aloft at the upper troposphere reinforced easterly vertical shear over north India. This increased shear may act to confine the Rossby wave response to the lower level and produce a stronger Ekman pumping–induced heating (Wang and Xie 1996; Xie and Wang 1996) and an enhanced meridional heat flux, both of which would increase the dynamic instability of the atmosphere and, thereby, increase monsoon precipitation.

Although the relationship between the two scenarios and the relative contribution from each scenario is unknown, given the relative weak intensity of the upstream CGT over Europe in June and July, the scenario I seems to be the dominate mechanism of the CGT in the early summer. However, in August and September, scenarios I and II may work together to establish the CGT. One possibility suggests that the ISM initially generates the downstream part of the CGT over Asia, the Pacific, and North America (scenario I), and the disturbance along the Atlantic jet excites an anomalous high over western Europe, which will produce the rest of the CGT over Europe and reinforce the ISM (scenario II). The other possibility is that the upstream CGT over Europe first triggers the ISM (scenario II), and the ISM, in turn, strengthens the anomalous high over west-central Asia and then generates the downstream part (scenario II).

We propose that a feasible mutually reinforced feedback between the CGT and ISM may provide a fruitful line of thinking for further research. First, the concurring change of precipitation and surface temperature on a global scale can be understood in terms of this teleconnection. Second, the midlatitude action center may also have a crucial influence on the ISM. Although the MJO and high-frequency intraseasonal oscillation originating from the equator are very important rainfall-producing mechanisms for the ISM, the potential influence of the midlatitude flow on northwest India and Pakistan is suggested. Third, similar to the WNPSM, the ISM also has a far-reaching impact on the east Asian and North American climate.

There are many ways in which the present study can be expanded. Clearly, much remains to be understood about the interaction between scenarios I and II. Substantial further progress on this issue will require a numerical simulation of the effect of the ISM and internal dynamic instability of basic state, and a better under-

standing of the interplay between the CGT and the ISM on the intraseasonal time scale. Such a study is currently under way and will be reported separately.

Acknowledgments. The authors wish to thank two anonymous referees' relevant comments that led to a much-improved manuscript. Section 6c was stimulated by one reviewer's comments. Thanks also are extended to Drs. S. P. Xie, F. F. Jin, T. Li, A. Barcilon, and Z. Wang for fruitful discussions. This study has been supported by the NSF climate dynamics program and NOAA/OGP Pacific and PACS programs.

REFERENCES

Ambrizzi, T., B. J. Hoskins, and H.-H. Hsu, 1995: Rossby wave propagation and teleconnection patterns in the austral winter. *J. Atmos. Sci.,* **52,** 3661–3672.

Barnston, A. G., and R. E. Livezey, 1987: Classification, seasonality and persistence of low-frequency atmospheric circulation patterns. *Mon. Wea. Rev.,* **115,** 1083–1126.

Branstator, G., 2002: Circumglobal teleconnections, the jet stream waveguide, and the North Atlantic Oscillation. *J. Climate,* **15,** 1893–1910.

Ding, Y.-H., 1992: Summer monsoon rainfalls in China. *J. Meteor. Soc. Japan,* **70,** 373–396.

——, 1994: *Monsoons over China.* Kluwer Academic, 419 pp.

Enomoto, T., B. J. Hoskins, and Y. Matsuda, 2003: The formation mechanism of the Bonin high in August. *Quart. J. Roy. Meteor. Soc.,* **129,** 157–178.

Feng, S., and Q. Hu, 2004: Variations in the teleconnection of ENSO and summer rainfall in northern China: A role of the Indian summer monsoon. *J. Climate,* **17,** 4871–4881.

Gill, A. E., 1980: Some simple solutions for heat induced tropical circulation. *Quart. J. Roy. Meteor. Soc.,* **106,** 447–462.

Guo, Q.-Y., and J.-Q. Wang, 1988: A comparative study on summer monsoon in China and India (in Chinese). *J. Trop. Meteor.,* **4,** 53–60.

Hoskins, B. J., and D. J. Karoly, 1981: The steady linear response of a spherical atmosphere to thermal and orographic forcing. *J. Atmos. Sci.,* **38,** 1179–1196.

——, and T. Ambrizzi, 1993: Rossby wave propagation on a realistic longitudinally varying flow. *J. Atmos. Sci.,* **50,** 1661–1671.

Joseph, P. V., and J. Srinivasan, 1999: Rossby waves in May and the Indian summer monsoon rainfall. *Tellus,* **51A,** 854–864.

Kalnay, E., and Coauthors, 1996: The NCEP/NCAR 40-Year Reanalysis Project. *Bull. Amer. Meteor. Soc.,* **77,** 437–471.

Kripalani, R. H., and S. V. Singh, 1993: Large-scale aspects of India–China summer monsoon rainfall. *Adv. Atmos. Sci.,* **10,** 72–84.

——, and A. Kulkarni, 1997: Rainfall variability over southeast Asia—Connections with Indian monsoon and ENSO extremes: New perspective. *Int. J. Climatol.,* **17,** 1155–1168.

——, and ——, 2001: Monsoon rainfall variations and teleconnections over south and east Asia. *Int. J. Climatol.,* **21,** 603–616.

——, ——, and S. V. Singh, 1997: Association of the Indian summer monsoon with the Northern Hemisphere mid-latitude circulation. *Int. J. Climatol.,* **17,** 1055–1067.

Krishnamurti, T. N., H. S. Bedi, and M. Subramaniam, 1989: The summer monsoon of 1987. *J. Climate,* **2,** 321–340.

Krishnan, R., and M. Sugi, 2001: Baiu rainfall variability and associated monsoon teleconnection. *J. Meteor. Soc. Japan,* **79,** 851–860.

Lau, K.-M., 1992: east Asian summer monsoon rainfall variability and climate teleconnection. *J. Meteor. Soc. Japan,* **70,** 211–240.

——, and H.-Y. Weng, 2002: Recurrent teleconnection patterns linking summertime precipitation variability over east Asia and North America. *J. Meteor. Soc. Japan,* **80,** 1309–1324.

——, K.-M. Kim, and J.-Y. Lee, 2004a: Interannual variability, global teleconnection and potential predictability associated with the Asian summer monsoon. *East Asian Monsoon*, C. P. Chang, Ed., World Scientific, 564 pp.

——, J.-Y. Lee, K.-M. Kim, and I.-S. Kang, 2004b: The North Pacific as a regulator of summertime climate over Eurasia and North America. *J. Climate,* **17,** 819–833.

Legates, D. R., and C. J. Willmott, 1990a: Mean seasonal and spatial variability global surface air temperature. *Theor. Appl. Climatol.,* **41,** 11–21.

——, and ——, 1990b: Mean seasonal and spatial variability in gauge-corrected, global precipitation. *Int. J. Climatol.,* **10,** 111–127.

Liang, P.-D., 1988: Indian summer monsoon and rainfall in North China in summer (in Chinese). *Acta Meteor. Sin.,* **46,** 75–81.

Liebmann, B., and D. L. Hartmann, 1984: An observational study of tropical–midlatitude interaction on intraseasonal time scales during winter. *J. Atmos. Sci.,* **41,** 3333–3350.

Lu, R.-Y., J.-H. Oh, and B.-J. Kim, 2002: A teleconnection pattern in upper-level meridional wind over the North African and Eurasian continent in summer. *Tellus,* **54A,** 44–55.

Mo, K. C., and R. E. Livezey, 1986: Tropical–extratropical geopotential height teleconnection during the Northern Hemisphere winter. *Mon. Wea. Rev.,* **114,** 2488–2515.

North, G. R., T. L. Bell, R. F. Cahalan, and F. J. Moeng, 1982: Sampling errors in the estimation of empirical orthogonal functions. *Mon. Wea. Rev.,* **110,** 699–706.

Ogi, M., K. Yamazaki, and Y. Tachibana, 2004: The summertime annular mode in the Northern Hemisphere and its linkage to the winter mode. *J. Geophys. Res.,* **109,** D20114, doi:10.1029/2004JD004514.

Parthasarathy, B., A. A. Munot, and D. R. Kothawale, 1994: All-India monthly and seasonal rainfall series 1871–1993. *Theor. Appl. Climatol.,* **49,** 217–224.

Preisendorfer, R. W., 1988: *Principal Component Analysis in Meteorology and Oceanography.* Elsevier, 425 pp.

Raman, C. R. V., and Y. P. Rao, 1981: Blocking highs over Asia and monsoon droughts over India. *Nature,* **289,** 271–273.

Ramaswamy, C., 1962: Breaks in the Indian summer monsoon as a phenomenon of interaction between the easterly and the subtropical westerly jet streams. *Tellus,* **14A,** 337–349.

Rodwell, M. J., and B. J. Hoskins, 1996: Monsoons and the dynamics of deserts. *Quart. J. Roy. Meteor. Soc.,* **122,** 1385–1404.

Sardeshmukh, P. D., and B. J. Hoskins, 1988: The generation of global rotational flow by steady idealized tropical divergence. *J. Atmos. Sci.,* **45,** 1228–1251.

Simmons, A. J., J. M. Wallace, and G. W. Branstator, 1983: Barotropic wave propagation and instability, and atmospheric teleconnection patterns. *J. Atmos. Sci.,* **40,** 1363–1392.

Thompson, D. W. J., and J. M. Wallace, 1998: The Arctic Oscillation signature in the wintertime geopotential height and temperature fields. *Geophys. Res. Lett.,* **25,** 1297–1300.

——, and ——, 2000: Annular modes in the extratropical circula-

tion. Part I: Month-to-month variability. *J. Climate,* **13,** 1000–1016.

Trenberth, K. E., G. W. Branstator, D. Karoly, A. Kumar, N.-C. Lau, and C. Ropelewski, 1998: Progress during TOGA in understanding and modeling global teleconnections associated with tropical sea surface temperatures. *J. Geophys. Res.,* **103** (C7), 14 291–14 324.

Wallace, J. M., and D. S. Gutzler, 1981: Teleconnections in the geopotential height field during the Northern Hemisphere winter. *Mon. Wea. Rev.,* **109,** 784–812.

Wang, B., and X.-S. Xie, 1996: Low-frequency equatorial waves in vertically sheared zonal flow. Part I: Stable waves. *J. Atmos. Sci.,* **53,** 449–467.

——, and Z. Fan, 1999: Choice of south Asian summer monsoon indices. *Bull. Amer. Meteor. Soc.,* **80,** 629–638.

——, R.-G. Wu, and K.-M. Lau, 2001: Interannual variability of the Asian summer monsoon: Contrasts between the Indian and the western North Pacific–east Asian monsoons. *J. Climate,* **14,** 4073–4090.

Wilks, D. S., 1995: *Statistical Methods in the Atmospheric Sciences: An Introduction.* Academic Press, 467 pp.

Wu, R.-G., and B. Wang, 2002: A contrast of the east Asian summer monsoon–ENSO relationship between 1962–77 and 1978–93. *J. Climate,* **15,** 3266–3279.

——, Z.-Z. Hu, and B. P. Kirtman, 2003: Evolution of ENSO-related rainfall anomalies in east Asia. *J. Climate,* **16,** 3742–3758.

Xie, X.-S., and B. Wang, 1996: Low-frequency equatorial waves in vertically sheared zonal flow. Part II: Unstable waves. *J. Atmos. Sci.,* **53,** 3589–3605.

Yang, S., K.-M. Lau, and K.-M. Kim, 2002: Variations of the east Asian jet stream and Asian–Pacific–American winter climate anomalies. *J. Climate,* **15,** 306–325.

Zhang, R.-H., 1999: The role of Indian summer monsoon water vapor transportation on the summer rainfall anomalies in the northern part of China during the El Niño mature phase (in Chinese). *Plateau Meteor.,* **18,** 567–574.